Kada HADDA [1,2], Amine BELOUFA [1], Mohamed AMIRAT [1],
Aissa BOUTTE [2]

Investigation on contact surfaces damage of copper contacts by an electric arc

Electrical contacts are used in general electrical applications such as circuit breakers, switches, relays, connectors, etc. Repeated separations of the parts (anode and cathode) of these contacts under input power can damage their contact materials. The objective of this work is to study the influence of the input electric power (100 W and 256 W) and the contact sizes (hemispherical contacts with diameters $D = 5$ mm and $D = 8$ mm) on the variation of the arc energy and the damage of the contact surfaces by oxidization or by erosion. These parameters are decisive for selecting the best arc-resistant contact sample. Experimental results, SEM, and EDX analysis show that high input power leads to more degradation of contact surfaces. Also, the smaller and the larger contact diameters generate similar arcing energies with similar erosion sizes and oxidation rates, but the contact with a small diameter has a higher lifetime (1215 operations) and oxidizes less quickly than the one with a large diameter that has a lower lifetime (374 operations). Experimental and numerical analyses demonstrate that arc mobility is one of several factors influencing the change in contact lifetime.

1. Introduction

Electrical connectors are used in many general applications (information technology, aeronautics, automotive, etc.), and our interest is to study the connectors used in automobiles. The pluggable connector contains two separable parts (anode and cathode) [1, 2].

✉ Amine BELOUFA, e-mail: beloufaamine@yahoo.fr

[1]Smart Structure Laboratory, University of Ain Temouchent, Ain Temouchent, Algeria

[2]Algerian Space Agency-Satellite Development Center Bir El Djir, Oran, Algeria

In the case of a closed contact, the two parts are in contact, and an electric current passes through it. When this connector is submitted to a high current, Joule heating will be generated in the closed contact surfaces, leading to an increase in the contact temperature that can cause melting of the contact surfaces. Since the Joule heat generation depends proportionally on the electrical contact resistance and the square of electric current (current fixed by the specifications and cannot be changed), the tendency then is to minimize electrical contact resistance; therefore, Joule heating and contact temperature. The authors [3–6] investigated the minimization of the electrical contact resistance of a closed power contact by acting on contact forces, contact shapes and geometries, contact materials, and the dimensions of connection cables.

This power contact is also exposed during its functioning to the vibration that can cause the corrosion of contact surfaces by fretting. Numerous researchers [7–9] studied this phenomenon to limit its devastating effect on power electrical contact.

In the case of a disconnection or an opening of the two contact parts under high voltage or high current, a phenomenon will appear. This phenomenon is the ignition of an electric arc between the anode and the cathode of the power contact. When the energy and temperature of this arc are high, they can damage contact surfaces and provoke heating, melting, high core temperature, erosion or welding, corrosion, and electrical insulating of contact surfaces after several opening-closing operations [10–14]. Damage of the contact material by the electric arc and the effect of the metal vapor on the net emission coefficient of the plasma, on the transport properties of the arc, and the contact material damage, are investigated by several researchers [15–20].

Electric arc has several negative consequences, such as generation of radiated electromagnetic interference [21, 22] that affects an electrical circuit or an electronic device by electromagnetic induction and can be detrimental to the functionality of this device. Arc can cause an increase in electrical contact resistance [23], fire, harmful radiation to the eyes, and no immediate interruption of the electric current in a circuit breaker either by the persistence of the arc between the relay contact terminals or by their welding, etc. In addition, arc fault or unintentional arc will have a disastrous effect if it is not well mastered. An arc can be affected by many factors, such as oxides, metal oxides, oxide films, gas environment (nitrogen, oxygen . . .), chemical gases, humidity, erosion, wear, etc. The presence of oil, grease, dust particles, or dirt on the contact surfaces can even influence the arc [24–26].

More investigations took place to minimize the disastrous effect of the electric arc on contact surfaces. The author [27] studied the electric arc and its consequences on contact surfaces of different electrodes, having a tip shape and a tip-flat shape with diverse sizes. A conclusion was drawn by [27] that an input power of 45 kW can lead to a faster erosion of the small electrode with an increase in gap distance. Also, the electrode with a tip shape facilitates arc initiation compared to an electrode with a tip-flat shape.

The author [28] compared the arc energy and arc duration for two contacts having pellet (pad) and rivet shapes; his results show that pellets that are somewhat

larger than rivets will allow high mobility of the arc. Another author [29] focused his work on producing next-generation contact materials in the form of nanostructured composites that will resist erosion by arc for various contacts in the form of rivets; [30–32] were interested in studying the influence of several contact materials on erosion by an arc of different contact shapes to select the most erosion-resistant material.

This paper aims to analyze the effect of the electric input power and the contact diameter of the degradation of the contact surfaces by an electric arc. In this work, an experimental study was carried out on electrical contact samples in the case of an opening contact; the material of these contacts is pure copper.

Contact samples have the same hemispherical contact shape with two different diameters (D = 5 mm and D = 8 mm) and are submitted to two input powers (P_{in} = 100 W and P_{in} = 256 W).

Through the previous papers, no one had studied contacts with the same shape and different sizes. For this reason, we are going to test different contact samples having the same shape with diverse sizes. Yet, in our experimental study, arc current, arc voltage, and arc duration are measured for several contact opening-closing operations. Arc power and arc energy were then deduced. A comparison between the results of the two applied electric powers and the two diameters of contact samples is presented in this paper to evaluate the predominant parameter that accelerates the degradation of the contact surfaces and consequently reduces the service lifetime of the contact. This experimental research is an original contribution to the science which had not been investigated before. It can concretize the hypothesis of the severity of arc mobility on the degradation of contact surfaces.

2. Shape and dimensions of the contact samples

Fig. 1 shows the dimensions in millimeters of the used hemispherical contacts. These contact samples are manufactured by ourselves. Two diameters of the hemi-

(a) Diameter of the hemispherical contact is equal to 5 mm

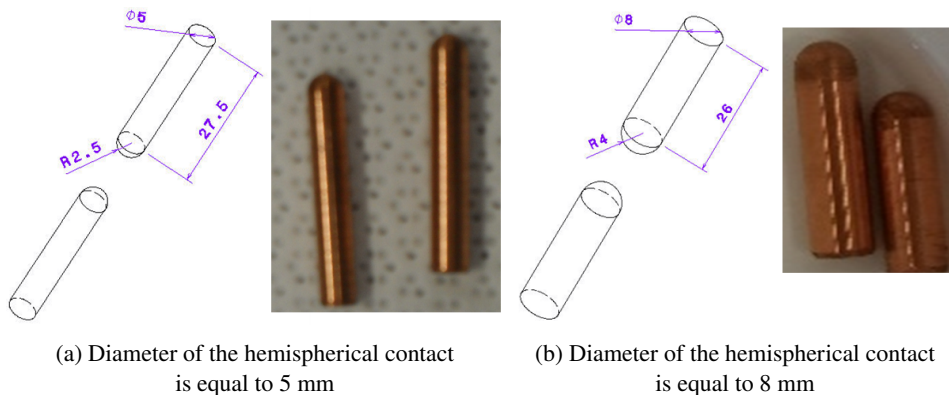(b) Diameter of the hemispherical contact is equal to 8 mm

Fig. 1. Dimensions of the used contact samples

spherical contact samples are tested; the first diameter is equal to 5 mm. However, the second is equal to 8 mm.

3. Materials of the tested contact samples

Table 1 presents the mechanical, electrical, and thermal properties of pure copper Cu 99.9% (the material of the tested contact samples). The choice fell on this material because pure copper is a classic material that does not contain any additional element. It is less expensive and has good thermoelectric and mechanical properties.

Table 1. Mechanical, thermal, and electrical properties of the pure copper material [1, 2]

Material	Cu 99.9%
Young modulus (GPa) at 20°C	124
Hardness (H_V) (MPa) at 20°C	400–900
Poisson ratio	0.33
Density (g/cm^3) at 20°C	8.92
Electrical resistivity at 20°C (Ωm)	16.8×10^{-9}
Electrical conductivity at 20°C ($\times 10^2$ Ω^{-1}mm^{-1})	595.2
Thermal conductivity at 20°C (W/mK)	394
Vapor pressure at melting point (Pa)	0.052
Specific heat of fusion J/kgK at 20°C	385

4. Experimental bench

Fig. 2 shows the experimental bench used to measure arc parameters (arc current and arc voltage) of our contact samples submitted to two DC input powers (100 W and 256 W). The experimental bench is composed of two parts: the first part is the mechanical system, and the second part is the electrical system. As shown in Fig. 2, the experimental bench is composed of two parts: the mechanical part and the electrical part.

4.1. Mechanical part of the experimental bench

The two contact parts are mounted on the jaws of the tensile testing machine named **Lloyd Instruments LS1**. The anode is fixed in the immobile lower jaw, whereas the cathode is fixed in the mobile upper jaw. To carry out the contact opening-closing operations (Fig. 2), a mobile crosshead ensures the movement of the ascent and descent of the cathode. Contact force is measured by a sensor having a precision of 0.01 N and a maximum measuring capacity of 1 kN. In our test, the
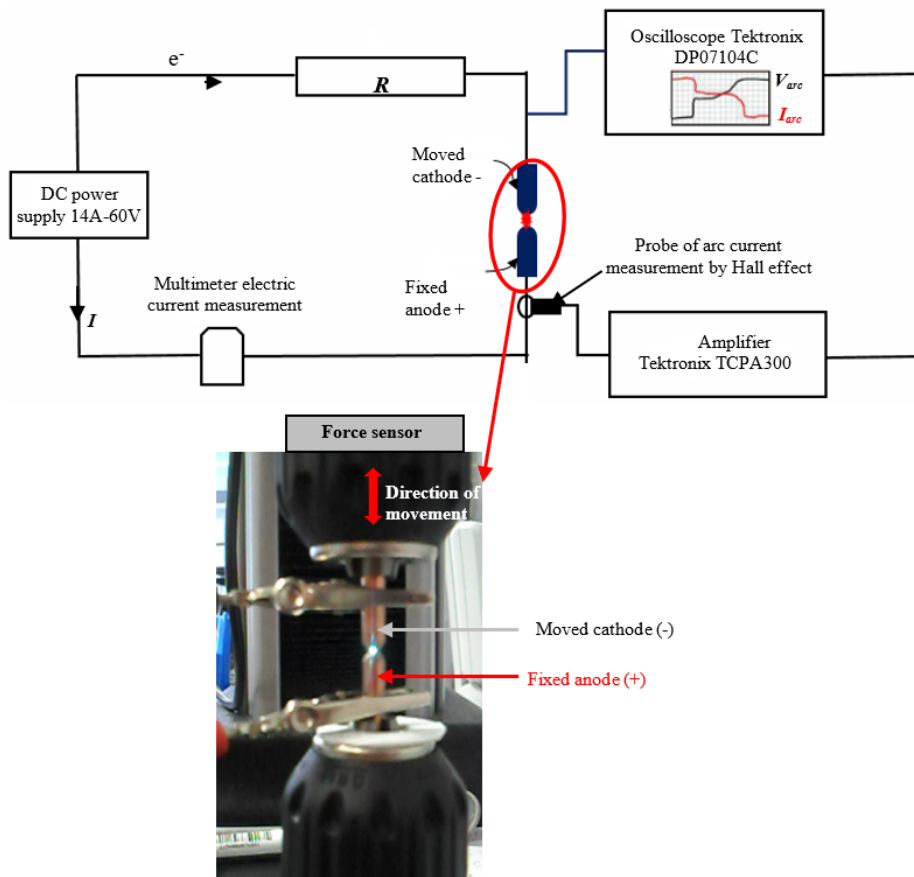
Fig. 2. Experimental bench for arc parameters measurement

applied contact force F_c is equal to 20 N while the opening velocity V_{open} is fixed to 5 mm/s.

An integrated displacement sensor is used to measure the displacement of the mobile jaw. During the entire test, the value of the opening gap d is fixed at 5 mm. This machine is monitored by a computer using the software *Nexygen-Plus*.

4.2. Electrical part of the experimental bench

A stabilized **TDK-Lambda ZUP60-7** power supply provides a maximum output current of 14 A with a maximum output voltage of 60V and a maximum electric power of 840 W. Firstly, in our case, the open voltage was fixed at 20 V with a DC current of 5A, which can give an input power of 100 W. Secondly, the voltage was fixed at 32 V with a DC current of 8 A, which can offer an input power of 256 W. The value of our invariable resistance is $R = 4\ \Omega$ (Fig. 2). A **Metrix Mx26** multimeter is used to measure and control the input current of the closed contact,

and to detect the separation of the electrodes; at this stage, the current will become zero. A **Tektronix DP07104C Digital Phosphor Oscilloscope** (1 GHz bandwidth, maximum sampling rate: 20 GSa/s) is used to measure during the contact opening the arc voltage with a voltage probe (500 MHz bandwidth and ×10 attenuation). For our test, the chosen sampling rate is equal to 1 MSa/s, allowing one measure by 1 µs; this is the time of one sampling period. The arc current is measured based on the Hall effect with a **Tektronix TCPA300** current probe amplifier (Fig. 2).

All the acquired data during one contact opening operation like the arc current and the arc voltage were processed later using a *Python* program to determine the arc duration, arc power, and arc energy for this operation. The acquisition of these data goes for all the opening-closing operations. The instrumentation and data collection part allow the automation of tests and the acquisition of data continuously. The bench is equipped with a portable PC connected directly to the machine via a USB interface; it is used for setting the test parameters such as the opening and closing speed, the applied contact force, the contact displacement, the opening gap, etc.

4.3. The adopted protocol to carry out our experimental tests

Before each experiment, the sample surfaces are cleaned with an alcohol bath to remove any dirt and insulating film present on the contact surfaces. Before starting the tests, the electrodes mounted in the machine's jaws must be aligned with high precision. We noticed that the severity of the arc during the contact closing is too low compared to that measured for the contact opening; the arc is almost extinguished during contact closure. For this reason, the electric current has not been cut off during the contact closure operations. It should be noted that contact opening-closing operations and the acquisition of results only stop until the end of the contact sample lifetime. All the tests were carried out at room temperature of 25°C and under atmospheric air having a moderate humidity with a pressure of 1 bar.

5. Results and discussion

5.1. Arc current I_{arc} and arc voltage V_{arc}

During all the tests, opening arc current I_{arc} and arc voltage V_{arc} are measured for all the opening-closing operations of the contact samples. For example, Fig. 3 shows, for operation number 300, the variation during the opening time of the I_{arc} and V_{arc} of the copper contact sample with a diameter D =5mm submitted to an input power P_{in} of 100 W. This power is equal to the open-voltage $V_0 = 20$ V multiplied by the applied DC current $I_0 = 5$ A. The arc voltage and current measurements on the break show fluctuations in their signals. These fluctuations are due to the variation during the time of the metal vapor pressure of the arc, which has been

diffused in the surrounding air near the contact zone [33] and [34]. Also, the density of the metal vapor plays a role in this fluctuation.
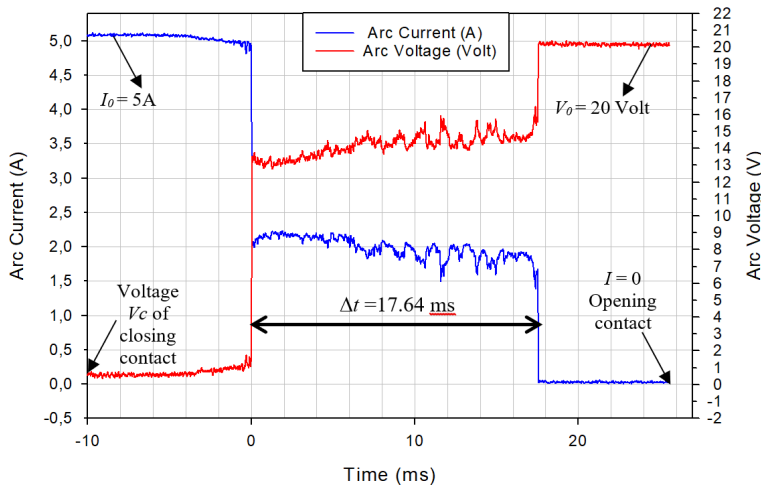

Fig. 3. Arc voltage V_{arc} and arc current I_{arc} for contact opening-closing operation N 300
($D = 5$ mm, $P_{\text{in}} = 100$ W)

One can conclude from the above figure that the variation of I_{arc} and V_{arc} is not linear. Various shapes of the electric arc are due to the nonlinearity of the arc current or the arc electric field. Arc always seeks the less resistive or more conductive path, even if it deforms. We can deduce from the latest figure an arc duration Δt equal to 17.64 ms.

5.2. Arc power P_{arc}, arc duration Δt & arc energy E_{arc}

From the two curves of I_{arc} and V_{arc} (Fig. 3), we can calculate the electric arc power $P_{\text{arc}}(t)$ by the following relation:

$$P_{\text{arc}}(t) = V_{\text{arc}}(t)\, I_{\text{arc}}(t). \tag{1}$$

The arc energy $E_{\text{arc}}(t)$ is calculated by the following relation:

$$E_{\text{arc}}(t) = \int P_{\text{arc}}(t)\,\mathrm{d}t = \int \left[V_{\text{arc}}(t)\, I_{\text{arc}}(t) \right] \mathrm{d}t. \tag{2}$$

Using equation (1), we can draw the variation of arc power during its arc duration for any opening operation. For example, Fig. 4 gives the change of arc power during the time for operation number 300 and for the two input powers 100 W and 256 W. The black curve presents the product of I_{arc} and V_{arc} illustrated previously in Fig. 3. One can see in the following figure (Fig. 4) that the arc power P_{arc} and the arc duration Δt vary proportionally with the input electric power P_{in}.
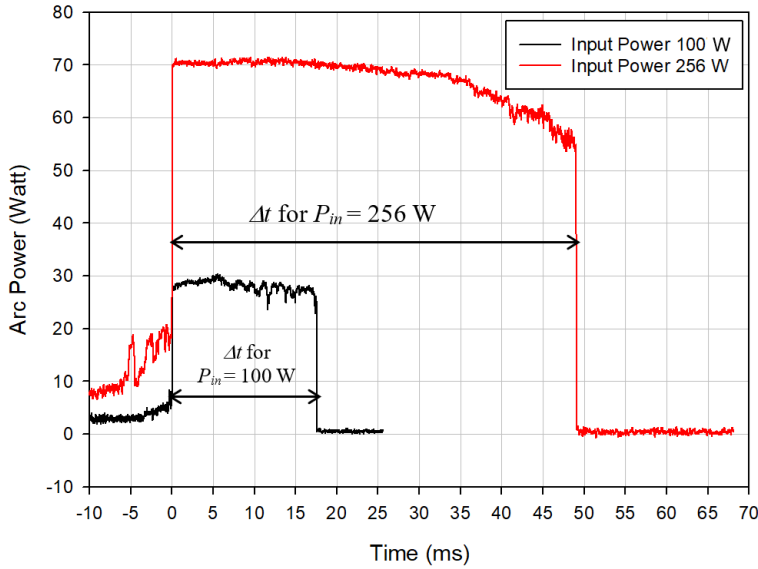
Fig. 4. Arc power for two input powers (D = 5 mm, P_{in} = 100 W and 256 W) (operation N 300)

From this figure (Fig. 4), we can also determine the maximum value of the arc power $P_{\text{arc}}^{\text{Max}}$.

Using $P_{\text{arc}}^{\text{Max}}$ and its corresponding arc duration Δt, the maximum arc energy can be calculated by:

$$E_{\text{arc}}^{\text{Max}} = P_{\text{arc}}^{\text{Max}}\Delta t. \tag{3}$$

For constant input power, the values of Δt and $P_{\text{arc}}^{\text{Max}}$ fluctuate during all the operations; this is due to the nature of the gas imprisoned between contact surfaces and its degree of ionization that depends on the temperature, humidity, pressure, . . . of this gas. Moreover, the fluctuation of Δt and $P_{\text{arc}}^{\text{Max}}$ is due to the morphology of the contact surfaces and the nature of the conductive layer material of these contact surfaces. It is interesting to note that there is no proportionality, from one operation to another, between the arc duration Δt and the maximum value of arc power. Consequently, our results will be analyzed by the maximum arc energy $E_{\text{arc}}^{\text{Max}}$ that contains the two previous terms Δt and $P_{\text{arc}}^{\text{Max}}$ (see equation (3)). After obtaining all the results of I_{arc}, V_{arc}, and P_{arc} for all the opening operations, we proceeded to calculate $E_{\text{arc}}^{\text{Max}}$ for each operation and plotted them in the following figure (Fig. 5) for the different test cases: contact samples with D = 5 mm submitted to input power of 100 W and 256 W, and contact samples with D = 8 mm submitted to the same input powers.

This figure (Fig. 5) shows a comparison between the maximum arc energies $E_{\text{arc}}^{\text{Max}}$ for the first 200 opening operations.

We can notice in the above figure that the maximum arc energy $E_{\text{arc}}^{\text{Max}}$ varies proportionally with the input electric power. In addition, for the same input power,
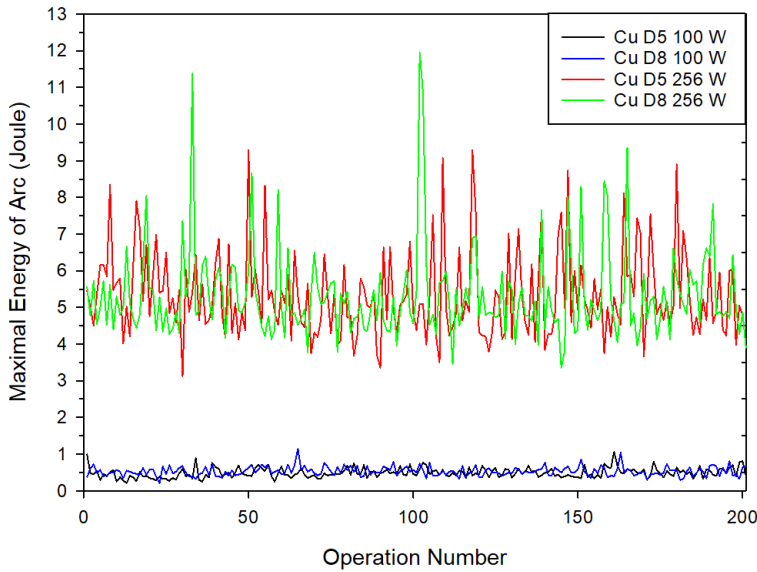
Fig. 5. Maximum arc energy for the two input powers (100 W and 256 W) and for the two diameters
(D = 5 mm and D = 8 mm)

the diameter of the contact sample does not influence the arc energy; there is not enough difference between the two arc energies for the two diameters D = 5 mm and D = 8 mm.

Table 2 gives the lifetime of various contact samples having different diameters submitted to different input powers; it shows a comparison between different averages of: Δt, $P_{\text{arc}}^{\text{Max}}$, and $E_{\text{arc}}^{\text{Max}}$. The maximum number of the opening operations n cited in this table corresponds to the last operation before the end service life of the contact. The contact reaches its end lifetime when its contact surfaces become electrically insulating.

Table 2. Different arc results for different contact samples

Diameter D (mm)	Input power P_{in} (Watt)	Maximum number of the opening operations (lifetime of the contact sample) n	Average of all Δt (ms)	Average of all $P_{\text{arc}}^{\text{Max}}$ (Watt)	Average of all $E_{\text{arc}}^{\text{Max}}$ (Joule)
5	100	13550	8.83	56.65	0.49
	256	1215	60.56	99.43	6.01
8	100	7019	8.14	57.39	0.45
	256	374	57.39	99.24	5.69

One can see in Table 2 that the contact sample with a large diameter has a lower lifetime compared to a contact sample with a small diameter. To understand

this phenomenon, we started to verify the cumulative frequencies of all the values of E_{arc}^{Max} for the two contacts.

Fig. 6 shows the cumulative frequency in the percentage of the operation numbers for a given interval of the E_{arc}^{Max} values.

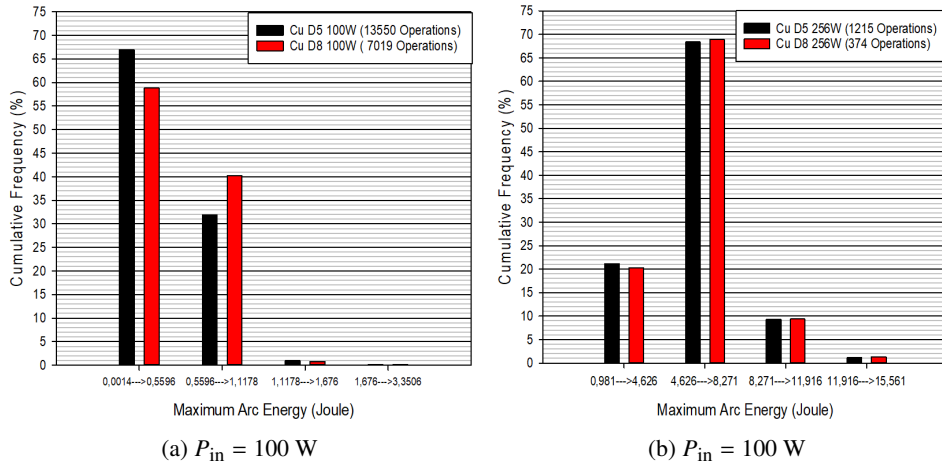(a) $P_{in} = 100$ W   (b) $P_{in} = 100$ W

Fig. 6. Histograms of the cumulative frequency versus maximum arc energy for contacts with diameters $D = 5$ mm and $D = 8$ mm submitted to two input powers

The cumulative frequency can be defined as the percentage of the number of opening operations that give values of E_{arc}^{Max} comprised in a given interval. This cumulative frequency is calculated with respect to the total number of operations n.

Take, for example, the histogram (Fig. 6a) corresponding to the power input of 100 W. In this example, E_{arc}^{Max} values lower than 0.56 Joule were obtained for 67% of n for the contact sample with a diameter $D = 5$ mm, while it is equal to 59% of n for the contact sample with a diameter $D = 8$ mm. Hence, for the two input powers and all the arc energy intervals, the cumulative frequency values for the two diameters ($D = 5$ mm and $D = 8$ mm) are not far away from one another (Fig. 6a and Fig. 6b). So, for any input power, the two contacts with diameters ($D = 5$ mm and $D = 8$ mm) have nearly the same arc energies (Fig. 5) and almost the same cumulative frequencies (Fig. 6). Thus, the last two parameters are not the ones that make the difference between the service lifetime for the two contact diameters ($D = 5$ mm and $D = 8$ mm); this leads us to the search for another factor that will make this difference.

We will carry out further investigations to better understand this phenomenon through analyzes of the damaged surfaces with microscopic, SEM, and EDX techniques.

5.3. Microscopic, SEM and EDX analyzes

Before giving detailed demonstrations on identifying the reason why the opening contact lifetime decreases with the increase in the hemispherical contact diameter, we are first going to provide some details on the influence of the input power on oxidation, erosion, and contact surface damage.

5.3.1. Oxidation of contact surfaces

The end lifetime of the contact sample corresponding to the last opening operation will occur when the contact surfaces become insulating, i.e., the contact surfaces don't transmit any electric current. At this stage, the contact surfaces are fully oxidized; this is confirmed by the analyses of the contact surfaces using SEM and EDX techniques (see Fig. 7).

Fig. 7 shows the mass proportions of the metal and the oxide present on the contact surfaces obtained at the end lifetime of our contact samples ($D = 5$ mm and $D = 8$ mm) submitted to an input power of 256 W. The measures have been held on contact surfaces using a scanning electron microscope SEM **JEOL JSM 6610LA**. From Fig. 7, an oxygen rate higher than 43% was obtained at the end of their lifetimes, except for the cathode with $D = 8$ mm, which means that its contact surface remains poorly conductive. EDX and SEM results indicate that the contact surfaces are oxidized and do not pass electric current. Furthermore, EDX spectra confirm the presence of the carbon element in the contact surfaces.

5.3.2. Influence of the input power on the contact lifetime

When the two contact electrodes start to move away from each other, a contact opening state will occur, and the contact area between the two electrodes decreases progressively. Hence, contact resistance, current density, and contact temperature increase, leading to the formation of molten metal bridge MMB between the contacts. After the rupture or the explosion of this bridge, a part of the exploded MMB transfers to the cathodic or the anodic contact causing the erosion of the contacts, and the other part of the exploded MMB participates in the formation of a very high-pressure, high-temperature metal vapor which releases electrons allowing the ionization of metal vapor (plasma) and the initiation of arc. In this arc, the DC electric current and energy are carried mainly by electrons and very little by metal and gas ions.

By the chemisorption process and at high arc temperature, the copper and the carbon existing on the contact surfaces absorb the air oxygen to form oxide layers on the contact surfaces. Both carbon dioxide CO_2 and carbon monoxide CO can be found and released from the contact surfaces [35] and [36]. Also, copper oxides CuO and Cu_2O have been seen on the contact surfaces. Note that the essential presence of carbon dioxide CO_2 and dioxygen O_2 initiates the copper oxidation reaction, which will be accelerated with the increase in temperature.
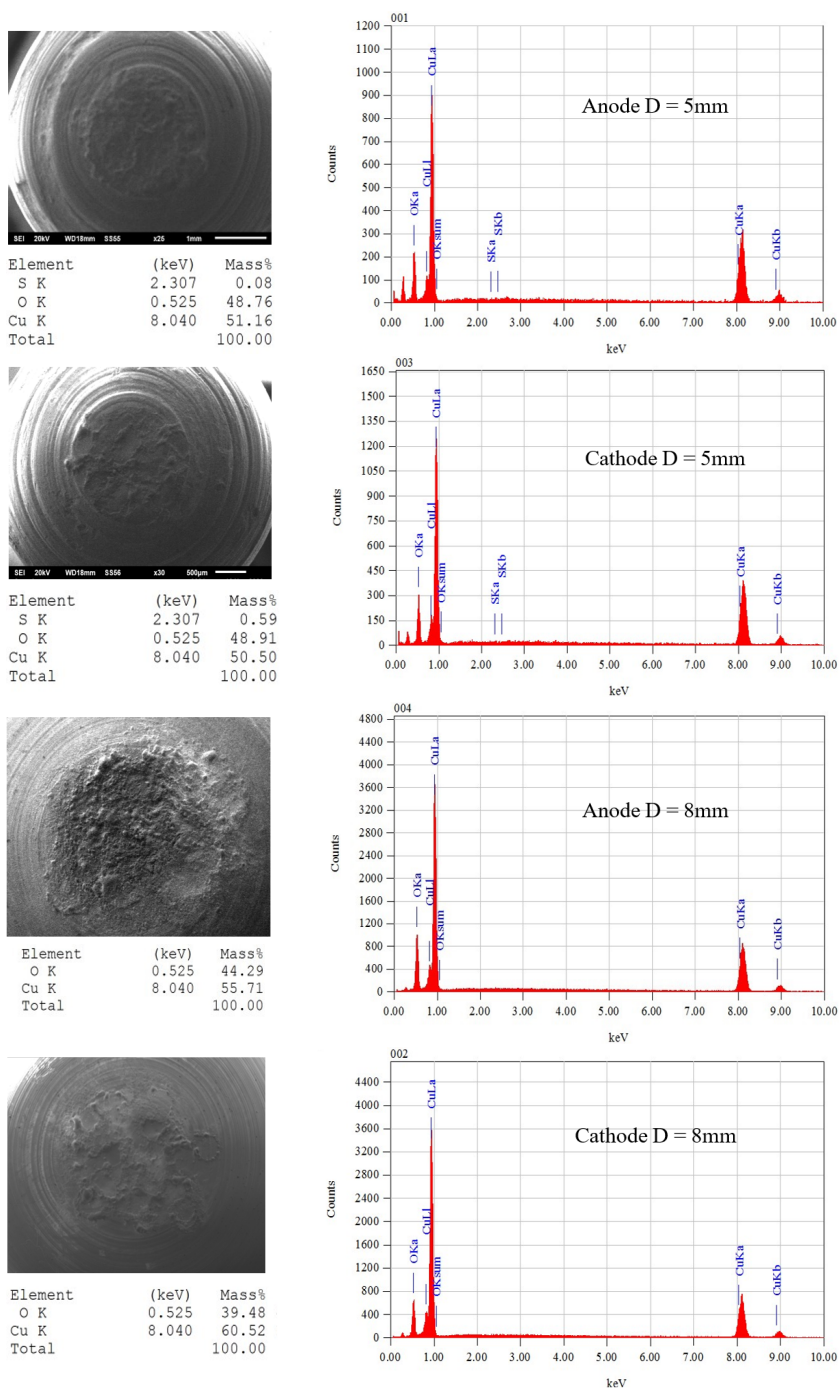
Element	(keV)	Mass%
S K	2.307	0.08
O K	0.525	48.76
Cu K	8.040	51.16
Total		100.00

Anode D = 5mm

Element	(keV)	Mass%
S K	2.307	0.59
O K	0.525	48.91
Cu K	8.040	50.50
Total		100.00

Cathode D = 5mm

Element	(keV)	Mass%
O K	0.525	44.29
Cu K	8.040	55.71
Total		100.00

Anode D = 8mm

Element	(keV)	Mass%
O K	0.525	39.48
Cu K	8.040	60.52
Total		100.00

Cathode D = 8mm

Fig. 7. Scanning Electron Microscopy (SEM) images and Energy Dispersive X-ray analysis (EDX) spectra of the chemical composition of the anode a nd cathode contact surfaces at the end of their lifetime (P_{in} = 256 W, D = 5 mm and 8 mm)

Referring to Table 2, we notice that for any diameter of the contact sample, the arc duration Δt, the maximum arc power P_{arc}^{Max}, and the maximum arc energy E_{arc}^{Max} increase with the increase of input power. Indeed, when the applied current I or voltage V increases, the input power also increases. Consequently, just after the opening operation, the electric field is very high, and contact surfaces heated by the Joule effect emit enough free electrons with high energy from the cathode to the anode. Also, these electrons will be accelerated by the high electric field. Therefore, we will have more collisions between electrons and gas ions. So, more ionization of the gas plasma will be confined between the contact surfaces, leading to high arc energy.

Yet, high arc energy provoked by high input power has a disastrous effect on the damage of the contact surfaces by oxidation and erosion. High input power or high arc energy induces high temperature in the contact material; therefore, the oxidation of the metallic contact surfaces will be accelerated by the rise of this temperature and will lead to a rapid failure of the contact (Table 2). In addition, high input power induces high arcing energy, leading to excessive degradation of the contact surfaces by erosion. Fig. 8 provides a comparison between contact surface images taken by an optical microscope at the end lifetime of the contact samples. These contacts have a diameter of $D = 5$ mm and are submitted to the two input powers 100 and 256 W. These images were taken on the anode and cathode parts of the contact. One can see that the contact surface submitted to an input power
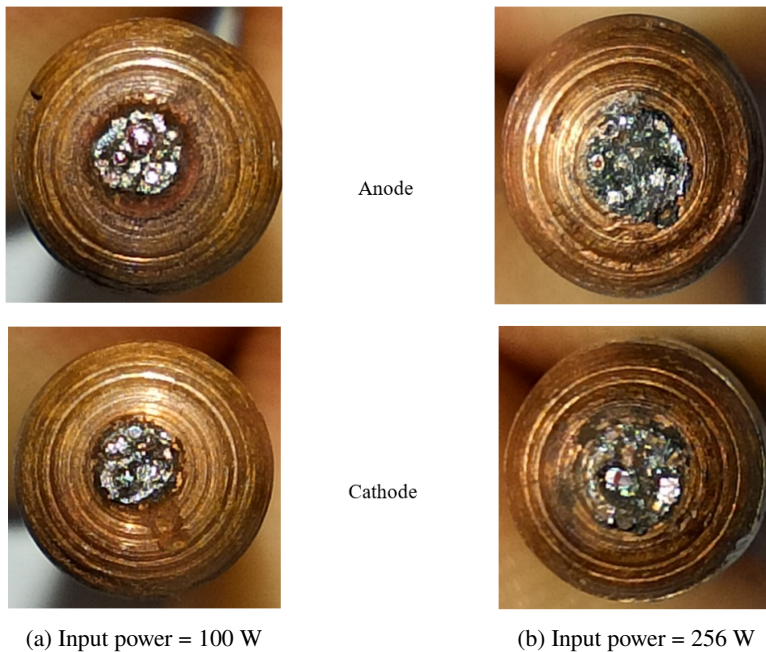

(a) Input power = 100 W	(b) Input power = 256 W

Fig. 8. Erosion of contact surfaces at the end of the contact lifetime (contacts with $D = 5$ mm, $P_{in} = 100$ W and 256 W)

of 256 W (Fig. 8b) is more eroded than the one submitted to an input power of 100 W (Fig. 8a). The same conclusion can be drawn for the contact with a diameter $D = 8$ mm. Also, we can see in the following figure (Fig. 8) that the black color in the eroded zones refers to the copper oxide CuO (Copper(II)), while the red-brown color refers to the oxide Cu_2O (Copper(I)).

5.3.3. Influence of the diameter of the hemispherical contact on the contact lifetime

For constant input power, the contact lifetime decreases with the increase of the contact diameter (see Table 2); this can be explained by the fact that if the diameter increases, the surface of the hemispherical part of the contact increases, and the arc will have more mobility on this surface, so more degradation. In fact, more demonstrations and arguments will be given later in the following paragraphs.

Fig. 9 gives a comparison between the sizes of the erosion zones for the contact parts of the ($D = 8$ mm and $D = 5$ mm). These erosion sizes were measured at the
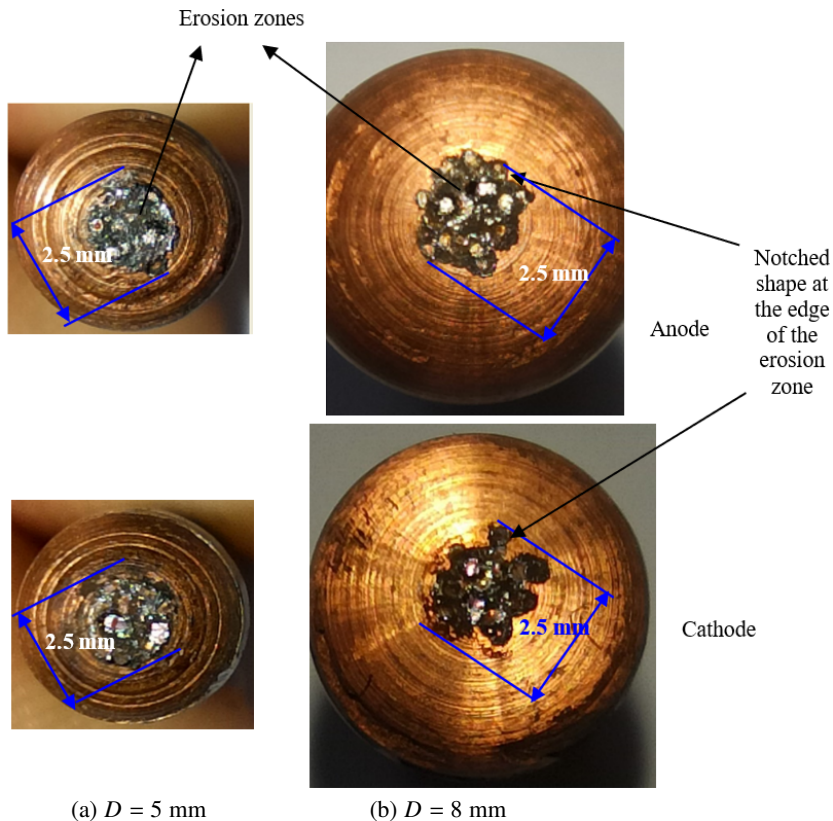

(a) $D = 5$ mm   (b) $D = 8$ mm

Fig. 9. Erosion of contact surfaces at the end of the lifetime of contacts ($D = 5$ mm and $D = 8$ mm, $P_{in} = 256$ W)

end of the lifetime of contacts; these contacts were submitted to an input power of 256 W. For the two contact samples (D = 8 mm and D = 5 mm), the diameter of the erosion zone is estimated to be near 2.5 mm. Therefore, the dimensions of the erosion zones are similar for the two contact samples. One can see in Fig. 9b, that the erosion zone for the contact sample with a diameter of 8 mm does not have a uniform circularity as the one obtained for a contact sample with a diameter of 5 mm. It was observed during all the opening operations that the arc makes turns with jumps on the contact surfaces for the contact sample with a diameter of 8 mm; this is confirmed by the presence of a notched shape at the edge of the erosion zone (Fig. 9b); this makes us think that the arc is more mobile for the contact sample with a diameter of 8 mm.

So, the two contacts submitted to identical input power (256 W) generate similar arc energies (Fig. 5) with almost the same erosion sizes (Fig. 9) and oxidation rates, while the contact sample with D = 5 mm has a lifetime of 1215 operations. However, the other one (with D = 8 mm) has a lifetime of 374 operations; this can confirm that the contact surface with D = 8 mm oxidizes rapidly compared to the contact with D = 5 mm.

During the experimental tests, we observed that the arc is too mobile for the contact with a diameter of 8 mm than the contact with a diameter of 5 mm. In fact, the arc mobility increases with the increase of the contact diameter because the arc is too mobile for the contact with a diameter of 8 mm; consequently, the struck point oxidizes rapidly by the hot free air, and the arc root seeks another less resistive path and strikes several random points with the principle of turn jumping (principal described previously in Fig. 9b). When all the points are oxidized, the contact surface of the arc mobility zone or the erosion zone becomes electrically insulating. Therefore, the contact reaches the end of its lifetime. One can conclude that the contact surface with D = 8 mm oxidizes rapidly by an arc too mobile compared to the contact with D = 5 mm. For this reason, the service lifetime of the contact with D = 8 mm is much lower than that of a contact with D = 5 mm. To confirm these experimental observations and conclusions concerning the arc mobility, a numerical MHD model was developed in the next section to calculate the arc mobility for the two contacts (D = 5 mm and D = 8 mm).

6. Numerical simulation of the arc for the two diameters (D = 5 mm and D = 8 mm)

To start, we give some theoretical notions on the arc motion. The arc mobility depends on the magnetic force $\vec{F}$ generated by the interaction between the induced magnetic field $\vec{B}$, and the current density $\vec{J}$. $\vec{B}$ is due to the arc motion and the passage of the electric current I inside the arc column (Fig. 10). The current that flows through the arc is I_{arc}. This current is the origin of the distribution of the electric current density $\vec{J}$ of the arc at the contact surfaces.

The relationship between the magnetic field $\vec{B}$ and the current density $\vec{J}$ gives birth to a term which is called the Lorentz magnetic force $\vec{F}$ (N/m³); the formula of this force is given by:

$$\vec{F} = \vec{J} \wedge \vec{B}. \tag{4}$$

Moreover, we can see in the above equation that the arc mobility force or the arc Lorentz force varies proportionally with the arc current density and the arc magnetic field; $\vec{J}$ (A/m²) and $\vec{B}$ (Tesla or $\mathrm{N\,m^{-1}A^{-1}}$) which depend on the applied current and the contact dimensions. Yet, the Ohm's law that defines the current density is given by:

$$\vec{J} = \frac{1}{\rho_{\mathrm{arc}}}\vec{E} = \sigma_{\mathrm{arc}}\vec{E} = \frac{I_{\mathrm{arc}}\,\vec{n}}{S_{\mathrm{arc}}}, \tag{5}$$

where $\vec{E}$ is the electric field (V/m), I_{arc} is the arc current (A), ρ_{arc} (Ωm) and σ_{arc} (S/m) are respectively the electrical resistivity and the electrical conductivity of the arc plasma gas, S_{arc} is the cross-sectional area of the arc column and $\vec{n}$ is the normal unit vector to the surface S_{arc}. Fig. 10 shows the arc mobility force or the arc Lorentz force created by the magnetic field once the current flows through the arc.

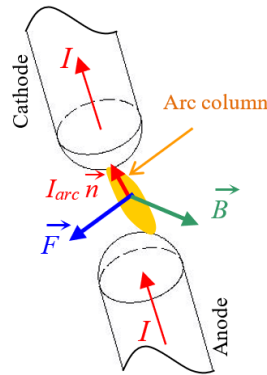Fig. 10. Magnetic field B, electric arc current I_{arc}, and Lorentz force F of the arc

The theoretical calculation of the current density distribution is laborious since we have no information about the dimensions of the arc column and its electrical conductivity. For this, we use the numerical calculation of this distribution using a 3D MHD numerical model developed by finite volume software (*Fluent V18.1*). This model can calculate the distribution of the arc electric current density $\vec{J}$ at the contact surfaces for the opening arcs of the two copper contacts ($D = 5$ mm and $D = 8$ mm) under an input power of 256W. The objective of the current density calculation is to see how the arc mobility force will vary through this density for the two contacts. The numerical results presented in the following figure (Fig. 11) confirm that the contact with a large diameter ($D = 8$ mm) has a higher distribution of the current density near the contact surfaces ($J_{\mathrm{D8}}^{\mathrm{Max}} = 5e+05$ A/m²) compared

to the contact with a small diameter ($D = 5$ mm) which has a maximum current density ($J_{D5}^{Max} = 4.05e+04$ A/m^2) (see the below Fig. 11); this high current density will generate a higher arc magnetic force which makes the arc too mobile.

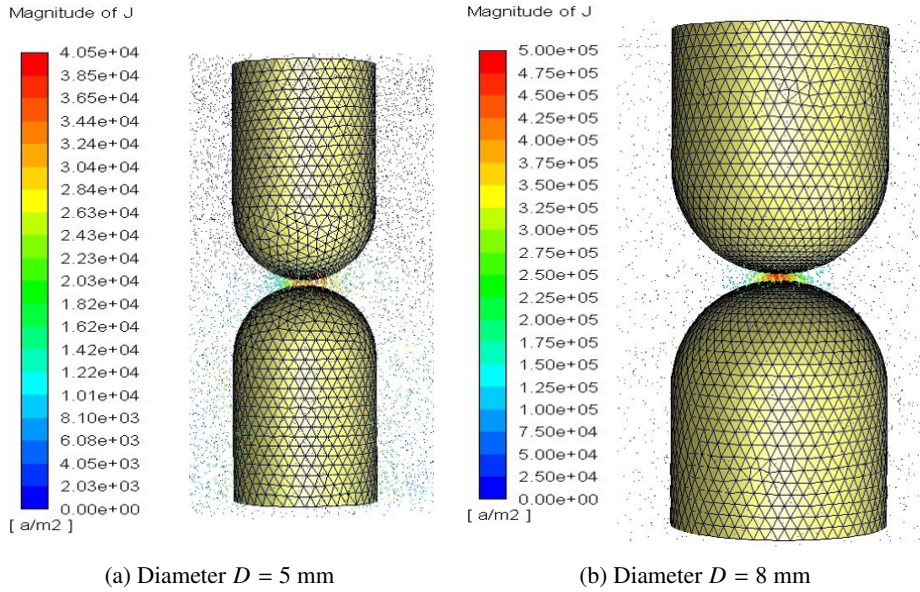(a) Diameter $D = 5$ mm   (b) Diameter $D = 8$ mm

Fig. 11. The distribution of the arc electric current density for the two contacts

As we have observed experimentally and demonstrated numerically, the mobility of the arc is higher for the contact with a large diameter. Consequently, we will have rapid oxidation for this contact. To explain the impact of this arc mobility on the degradation of contact surfaces, we have presented in the following figure the difference between the arc mobility for the two contact samples ($D = 5$ mm and $D = 8$ mm) and its consequence on the degradation of contact surfaces.

For the contact with diameter $D = 5$ mm (Fig. 12a), the arc strikes the same black target point from the first to the N-th operation (N can reach 25 operations or more); this point remains conductive (i.e., not oxidized) until the N-th operation. After this operation, the first struck point oxidizes, and the arc does not pass through this point. The arc seeks another less resistive path that corresponds to another point very close to the first point (Fig. 12a). On the other hand, for the contact with a diameter $D = 8$ mm (Fig. 12b), the arc is too mobile; it strikes several random points with the principle of turn jumping (principal described previously in Fig. 9b), and with a frequency of two to three operations for each point, a frequency much lower than that observed for the contact with a diameter $D = 5$ mm; this leads to rapid oxidation of the first struck point by the hot free air. Hence, the other points oxidize one after the other (Fig. 12b). When all the points are oxidized, the contact surface of the arc mobility zone or the erosion zone becomes electrically insulating. Therefore, the contact reaches the end of its lifetime. One can conclude

that the contact surface with $D = 8$ mm oxidizes rapidly by an arc too mobile compared to the contact with $D = 5$ mm. For this reason, the service lifetime of the contact with $D = 8$ mm is much lower than that of a contact with $D = 5$ mm.
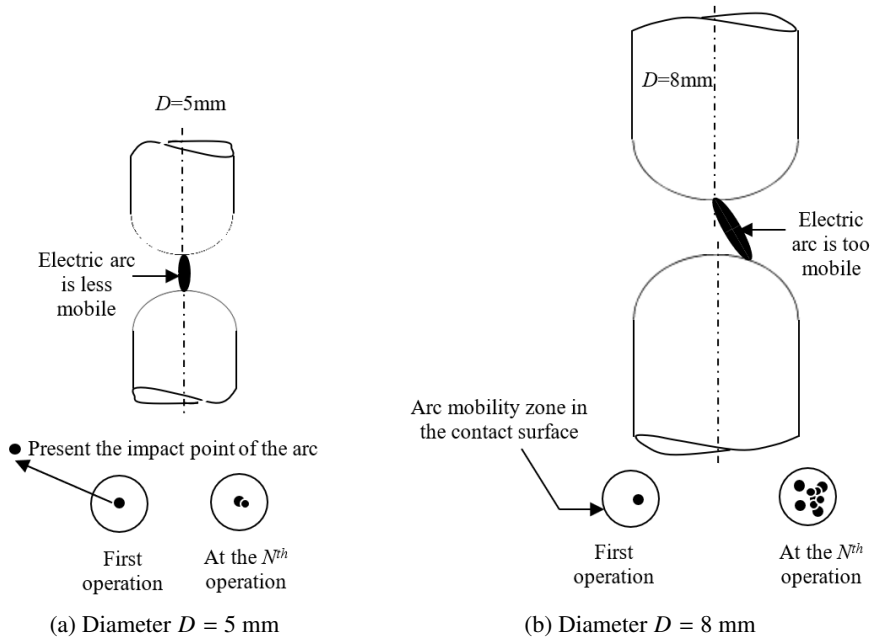

(a) Diameter $D = 5$ mm   (b) Diameter $D = 8$ mm

Fig. 12. Arc mobility impact on the degradation of the contact zone of the two contact samples ($D = 5$ mm and $D = 8$ mm)

7. Conclusion

During the opening-closing operations, the service lifetime of an electrical contact sample depends on the severity of the arc and its energy. High arc energy leads to erosion, oxidation, and electric insulation of contact surfaces. The total erosion of the contact interfaces is a combination of material transfer, material vaporization, mechanical damage caused by the impact of the two contact parts, material fatigue, wear, and the separation of the welded surfaces.

In this research paper, the impact of this arc on the damage of the contact surfaces has been studied for hemispherical contact samples having two different diameters ($D = 5$ mm and $D = 8$ mm) and submitted to two input powers 100 W and 256 W. Through this research paper, some interesting conclusions have been obtained. It was shown that for any contact diameter, the arc energy is more influenced by the input power; high input power leads to high arc energy, high arc duration, high oxidation and erosion, and low service lifetime. SEM and EDX results confirm that the failure of the contact sample will occur when the oxygen

rate in the eroded contact surface exceeds 43% (i.e., when this surface becomes oxidized). It was concluded that the two contacts with two diameters (D = 5 mm and D = 8 mm), which are submitted to an identical input power generate similar arcing energies with almost the same cumulative frequencies. These contacts have nearly the same erosion sizes and oxidation rates; whereas a contact with a small diameter has a higher lifetime compared to one with a large diameter whatever the input power.

It has been explained with the help of our numerical calculations and experimental observations that contact with large diameter has high arc mobility; this accelerates the oxidation of the contact surfaces and leads to a rapid decrease in the contact lifetime; this leads us to say that an opening contact with a small diameter has better electric arc resistance than one with a large diameter, which is the opposite of a closed contact where contact with a large diameter is preferred over contact with a small diameter because its electrical contact resistance is low.

Finally, the combined usage of contact with a large diameter submitted to a high input power provokes high arc energy with a high temperature and arc mobility. All these lead to rapid degradation and damage of the contact surfaces by oxidation, ultimately resulting in the device failure. Since copper is less expensive than noble materials, the ability to use it in power opening contacts in the form of a hemispherical contact with a small diameter is more interesting for manufacturers of electric opening connectors.

Acknowledgements

References

[1] R. Holm. *Electric Contacts: Theory and Application*. Springer-Verlag, Berlin, 1981.

[2] P.G. Slade. *Electrical Contacts: Principles and Applications*. CRC Press, New York, 2014.

[3] A. Beloufa. *Numerical and experimental analysis of the electrical, mechanical and thermal behavior of electrical contacts in the fields of forces (1 to 100 N) and currents (1 to 100 A). Analyse numérique et expérimentale du comportement électrique, mécanique et thermique des contacts électriques dans les domaines de forces (1 à 100 N) et de courants (1 à 100 A)*. Ph.D. Thesis, University of Rennes, Rennes, France, 2008 (in French).

[4] A. Beloufa. The effect of cable section on the variation of power automotive connector temperature. *IEEE Transactions on Components, Packaging and Manufacturing Technology*, 9(6):1020–1028, 2019. doi: 10.1109/TCPMT.2019.2914894.

[5] A. Beloufa, and M. Amirat. Design and study of new power connector with parallel contact points. *Proceeding of the Institution of Mechanical Engineers Part D: Journal of Automobile Engineering*, 232(14):2014–2021, 2018. doi: 10.1177/0954407018764146.

[6] A. Beloufa. Design optimization of electrical power contact using finite element method. *ASME Journal of Heat Transfer*, 134(1):011401, 2012. doi: 10.1115/1.4004713.

[7] A. Beloufa. Conduction degradation by fretting corrosion phenomena for contact samples made of high-copper alloys. *Tribology International*, 43(11):2110–2119, 2010. doi: 10.1016/j.triboint.2010.06.006.

[8] A. Beloufa. Investigation on contact surface damage of automotive connector by fretting corrosion. In: M. Hadfield, C.A. Brebbia, J. Seabra, (eds.): *Tribology and Design*, pages 141–154. WIT Transactions on Engineering Sciences, WIT Press, 2010. doi: 10.2495/TD100131.

[9] H. Yang and I. Green. Mitigation schemes for the reduction of fretting wear and fatigue. In: *2021 IEEE 66th Holm Conference on Electrical Contacts (HLM)*, pages 51–56, San Antonio, USA, 24-27 Oct.2021. doi: 10.1109/HLM51431.2021.9671166.

[10] P.G. Slade. The Transition from to the metallic phase arc after the rupture of the molten metal bridge for contacts opening in air and vacuum. In: *2008 Proceeding of the 54th IEEE Holm Conference on Electrical Contacts*,pages 1–8, Orlando, USA, 27-29 Oct. 2008. doi: 10.1109/HOLM.2008.ECP.14.

[11] L. Doublet, N.B. Jemaa, F. Hauner, and D. Jeannot. Make arc erosion and welding tendency under 42 VDC in automotive area. In: *Proceeding of the 49th IEEE Holm Conference on Electrical Contacts*, pages 158–162, Washington, DC, USA, 08-10 Sept. 2003. doi: 10.1109/HOLM.2003.1246492.

[12] S.N. Kharin and M.M. Sarsengeldin. The role of the arc flux and Joule heating in the erosion of electrical contacts. In: *2017 IEEE Holm Conference on Electrical Contacts*, pages 293–301, Denver, USA, 10-13 Sept. 2017. doi: 10.1109/HOLM.2017.8088102.

[13] F. Pons. *Electrical contact material arc erosion: experiments and modeling towards the design of an AgCdO substitute*. Ph.D. Thesis, Georgia Institute of Technology, USA, 2010.

[14] A. Bonhomme. *Wear behavior of the electrical contact pads mad with silver matrix*. Ph.D. Thesis, Paris Mining School, Paris, France, 2005 (in French).

[15] J.J. Lowke, R. Morrow, and J. Haidar. A simplified unified theory of arcs and their electrodes. *Journal of Physics D: Applied Physics*. 30(14):2033–2042, 1997. doi: 10.1088/0022-3727/30/14/011.

[16] M. Tanaka, K. Yamamoto, S. Tashiro, K. Nakata, E. Yamamoto, K. Yamazaki, K. Suzuki, A.B. Murphy, and J.J. Lowke. Time-dependent calculations of molten pool formation and thermal plasma with metal vapour in gas tungsten arc welding. *Journal of Physics D: Applied Physics*, 43(43):434009, 2010. doi: 10.1088/0022-3727/43/43/434009.

[17] Y. Liu, A. Guha, J. Montanyà, Y. Wang, and Z. Fu. Effects of single impulse current and multiwaveform multipulse currents on aluminum alloy in lightning damage analysis. *IEEE Transactions on Plasma Science*, 48(4):1146–1153, 2020. doi: 10.1109/TPS.2020.2977930.

[18] Y. Liu and Y. Wang. Is indirect electrode a good choice for simulated lightning damage tests? – The effect of metal vapor. *IEEE Transactions on Plasma Science*, 49(5):1661–1668, 2021. doi: 10.1109/TPS.2021.3073534.

[19] S.L. Millen, A. Murphy, G. Abdelal, and G. Catalanotti. Sequential finite element modelling of lightning arc plasma and composite specimen thermal-electric damage. *Computers & Structures*, 222:48–62, 2019. doi: 10.1016/j.compstruc.2019.06.005.

[20] Y. Liu and Y. Wang. Modeling the lightning continuing current electric arc discharge and material thermal damage: Effects of combinations of amplitude and duration. *International Journal of Thermal Sciences*, 162:106786, 2021. doi: 10.1016/j.ijthermalsci.2020.106786.

[21] Y. Wang et al. Characterization and measurement method of DC arc electromagnetic radiation for photovoltaic systems. *Transactions of China Electrotechnical Society*, 34(14):2913–2921, 2019. doi: 10.19595/j.cnki.1000-6753.tces.180711. (in Chinese).

[22] F. Karetta, and M. Lindmayer. Simulation of the gasdynamic and electromagnetic processes in low voltage switching arcs. In: *Proceeding of the 42nd IEEE Holm Conference on Electrical Contacts*, pages 35–44,Chicago, USA, 16-20 Sept. 1996. doi: 10.1109/HOLM.1996.557177.

[23] P.G. Slade. Effect of the electric arc and the ambient air on the contact resistance of silver, tungsten, and silver-tungsten contacts. *Journal of Applied Physics*, 47(8):3438–3443, 1976. doi: 10.1063/1.323181.

[24] D. Grogg, and C. Schrank. Impact of the gas environment on the electric arc. In: *2016 IEEE 62nd Holm Conference on Electrical Contacts*, pages 125–128, Clearwater Beach, USA, 09-12 Oct. 2016. doi: 10.1109/HOLM.2016.7780019.

[25] P. Verma, O.P. Pandey, and A. Verma. Influence of metal oxides on the arc erosion behaviour of silver metal oxides electrical contact materials. *Journal of Materials Science & Technology*, 20(1):49–54, 2004.

[26] J.F. Llewellyn. The physics of electrical contact phenomena. *British Journal of Applied Physics*, 12(7):318–322, 1961. doi: 10.1088/0508-3443/12/7/302.

[27] A. Farhadi, Y. Zhu, L. Gu, and W. Zhao. Influence of electrode shape and size on electric arc channel and crater. *Procedia CIRP*, 68:215–220, 2018. doi: 10.1016/j.procir.2017.12.051.

[28] E. Yee Kin Choi. *Study of arcs and their consequences on electrical power contact materials for DC applications*. Ph.D. Thesis, University of Rennes, Rennes, France, 2015 (in French).

[29] S. Księżarek, M. Woch, D. Kołacz, M. Kamińska, P. Borkowski, and E. Walczuk. Progress in fabrication technology of silver-based contact materials with particular account of the Ag-Re and Ag-SnO2Bi2O3 composites. *Archives of Metallurgy and Materials*, 59(2):501–508, 2014. doi: 10.2478/amm-2014-0083.

[30] M. Mohammadhosein, K. Niayesh, A.A.S. Akmal, and H. Mohseni. Impact of surface morphology on arcing induced erosion of CuW contacts in gas circuit breakers. In: *2018 IEEE Holm Conference on Electrical Contacts*, pages 99–105, Albuquerque, USA, 14-18 Oct. 2018. doi: 10.1109/HOLM.2018.8611731.

[31] M. Abbaoui, A. Lefort, D. Sallais, and N.B. Jemaa. Theoretical and experimental determination of erosion rate due to arcing in electrical contacts. In: *Proceeding of the 52nd IEEE Holm Conference on Electrical Contacts*, pages 103–109, Montreal, Canada, 25-27 Sept. 2006. doi: 10.1109/HOLM.2006.284072.

[32] D. Sallais, N.B. Jemaa, and E. Carvou. An arc study at high DC current levels in automotive applications. *IEEE Transactions on Components, Packaging and Manufacturing Technology*, 30(3):540–545, 2007. doi: 10.1109/TCAPT.2007.903499.

[33] N.B. Jemaa, J.L. Queffelec, and D. Travers. Some investigations on slow and fast arc voltage fluctuations for contact materials proceeding in various gases and direct current. In: *Thirty-Sixth IEEE Conference on Electrical Contacts*, pages 18–24, Montreal, Canada, 1990. doi: 10.1109/HOLM.1990.112989.

[34] P.J. Boddy and T. Utsumi. Fluctuation of arc potential caused by metal-vapor diffusion arcs in air. *Journal of Applied Physics*, 42(9):3369–3373, 1971. doi: 10.1063/1.1660739.

[35] J.D. Lambert. The oxidation of carbon. *Transactions of the Faraday Society*, 32:452–462, 1936.

[36] D.Y. Cho, K.J. Kim, K.S. Lee, M. Lübben, S. Chen, and I. Valov. Chemical influence of carbon interface layers in metal/oxide resistive switches. *ACS Applied Materials & Interfaces*, 15(14):18528–18536, 2023. doi: 10.1021/acsami.3c00920.